



End Report

Neel B. Rambhia
Indian Institute of Technology Bombay

Undergraduate Research Internship
May 9, 2024 - July 12, 2024

Guide: Prof. Andrew Wing On POON
Mentors: Qianni Zhang, Jiantao Wang



Photonics Device Laboratory
Dept. of Electronic and Computer Engineering
The Hong Kong University of Science and Technology

Chapter 1

Hang - Ou - Mandel Effect

1.1 Introduction

The Hong-Ou-Mandel (HOM) effect is a demonstration of quantum interference, where two indistinguishable photons incident on a beam splitter exhibit a unique correlation in their detection. This effect is pivotal in quantum optics and quantum information processing, providing insights into the nature of quantum states and their interactions.

1.2 Theoretical Background

1.2.1 Quantum Interference

Quantum interference arises when the probability amplitude of indistinguishable quantum states overlap, leading to observable interference patterns. This phenomenon is crucial in understanding two-photon interference effects.

In classical wave interference, the intensity of the resultant wave is determined by the superposition of individual wave amplitudes. Similarly, in quantum mechanics, the probability amplitude of different paths taken by quantum particles can interfere. The resultant probability is given by the square of the sum of the probability amplitudes.

1.2.2 Two-Photon Interference

Two-photon interference occurs when two photons are superposed, resulting in the interference of their probability amplitudes. This principle underlies the HOM effect. When two indistinguishable photons are incident on a beam splitter, their paths become entangled, and their joint detection probability exhibits interference fringes.

1.3 The Hong-Ou-Mandel Effect

1.3.1 Basic Setup

The typical HOM setup involves a 50:50 beam splitter and two single-photon sources. The photons are directed towards the beam splitter, and detectors are placed at the output ports. The beam splitter has the property of splitting an incident photon into two paths with equal probability.

1.3.2 Quantum State of the Photons

Consider two indistinguishable photons entering the beam splitter from ports A and B. The initial state of the system is given by

$$|\psi_{\text{in}}\rangle = |1_A\rangle|1_B\rangle,$$

where $|1_A\rangle$ and $|1_B\rangle$ represent single-photon states in modes A and B, respectively.

After passing through the beam splitter, the state transforms according to the beam splitter transformation rules:

$$|1_A\rangle \rightarrow \frac{1}{\sqrt{2}}(|1_C\rangle + |1_D\rangle),$$

$$|1_B\rangle \rightarrow \frac{1}{\sqrt{2}}(|1_C\rangle - |1_D\rangle).$$

Using the tensor product to combine the states, the output state becomes

$$|\psi_{\text{out}}\rangle = \frac{1}{\sqrt{2}}(|1_C\rangle + |1_D\rangle) \otimes \frac{1}{\sqrt{2}}(|1_C\rangle - |1_D\rangle).$$

Expanding this, we get

$$|\psi_{\text{out}}\rangle = \frac{1}{2} (|2_C\rangle|0_D\rangle + |0_C\rangle|2_D\rangle - |1_C\rangle|1_D\rangle + |1_C\rangle|1_D\rangle).$$

Simplifying the terms, we find

$$|\psi_{\text{out}}\rangle = \frac{1}{2} (|2_C\rangle|0_D\rangle + |0_C\rangle|2_D\rangle),$$

since the $|1_C\rangle|1_D\rangle$ terms cancel out.

1.3.3 Coincidence Probability

The coincidence probability is derived by considering the probability amplitude of detecting one photon at each output port. For indistinguishable photons, the probability amplitudes interfere destructively, leading to

$$P_{\text{coinc}} = |\langle 1_C | \langle 1_D | \psi_{\text{out}} \rangle|^2 = 0.$$

This zero probability of coincidence detection is the hallmark of the HOM effect.

When the photons are distinguishable, the interference pattern is lost, and the coincidence probability is

$$P_{\text{coinc}} = \left| \langle 1_C | \langle 1_D | \frac{1}{\sqrt{2}}(|1_C\rangle|1_D\rangle + |1_D\rangle|1_C\rangle) \right|^2 = \frac{1}{2}.$$

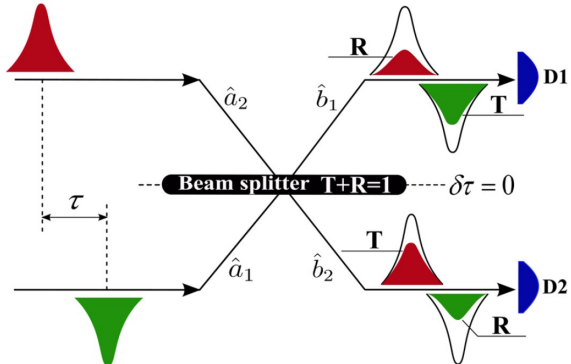
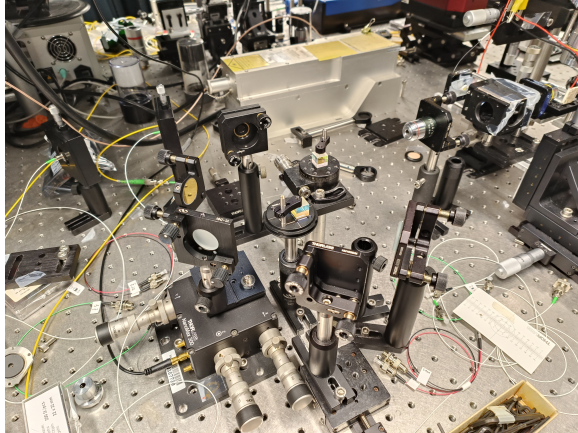


Figure 1.1: Left: Hong-Ou-Mandel setup @ Photonics Device Lab, HKUST. Right: Schematic representation of the HOM interferometer, where D_1, D_2 are the first and second detectors, respectively; τ is the time delay between 1 and 2 photons and $\delta\tau$ is the time delay caused by the spatial displacement of the BS from the equilibrium position [1]

1.4 Experimental Realization

The HOM effect has been experimentally realized using various types of single-photon sources, such as spontaneous parametric down-conversion (SPDC) and quantum dots. The setup typically involves precise timing and synchronization of photon arrival times to ensure indistinguishability.

In SPDC, a nonlinear crystal is pumped with a laser to produce photon pairs. These pairs are then directed towards the beam splitter. By adjusting the path lengths and using delay lines, the arrival times of the photons can be synchronized.

My work involved setting up the different parts of the HOM setup and tuning them carefully to align them together, testing the interference of each of the detectors and convergence of the lenses used in the setup. The testing was done for two specific range of wavelengths centred at 780 nm and 1550 nm with the span of 10 nm - 15 nm.

Chapter 2

Notch Type Ring Resonators

2.1 Introduction

Ring resonators are critical components in photonic circuits, offering applications in filtering, sensing, and modulation. Among various configurations, notch-type ring resonators are notable for their unique filtering characteristics. This report focuses on the fundamental aspects of notch-type ring resonators, including their structure, operation, and derivations of key equations governing their behavior.

2.2 Ring Resonator Structure

2.2.1 Basic Configuration

The basic configuration of a ring resonator consists of a waveguide coupled to a ring waveguide of radius r . The coupling mechanism is typically unidirectional, ensuring that a single mode is excited within the resonator. The setup assumes lossless coupling, single polarization, and no cross-coupling between different polarization modes.

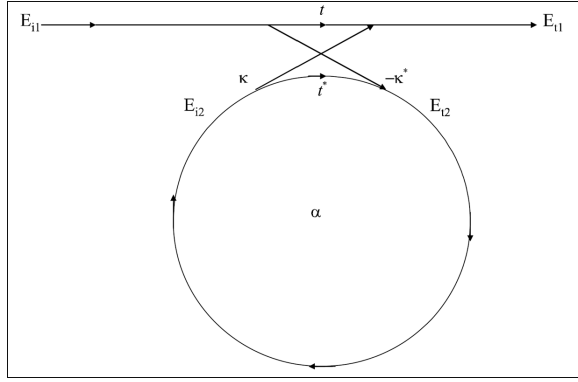


Figure 2.1: Basic configuration of a ring resonator coupled to a waveguide [2]

2.2.2 Mathematical Model

The interaction in the ring resonator can be described by the matrix relation:

$$\begin{pmatrix} E_{t1} \\ E_{t2} \end{pmatrix} = \begin{pmatrix} t & \kappa \\ -\kappa^* & t^* \end{pmatrix} \begin{pmatrix} E_{i1} \\ E_{i2} \end{pmatrix} \quad (2.1)$$

where E represents the complex mode amplitudes, normalized such that their squared magnitude corresponds to the modal power. The parameters t and κ are the coupler parameters, with t being the transmission coefficient and κ the coupling coefficient. These parameters satisfy the condition:

$$|\kappa|^2 + |t|^2 = 1 \quad (2.2)$$

2.3 Operation Principle

2.3.1 Round Trip Analysis

Assuming $E_{i1} = 1$, the round trip in the ring is given by:

$$E_{i2} = \alpha \cdot e^{j\theta} E_{t2} \quad (2.3)$$

where α is the loss coefficient (with $\alpha = 1$ for zero loss) and θ is the phase shift given by:

$$\theta = \frac{\omega L}{c} = \frac{2\pi r \cdot n_{\text{eff}}}{\lambda} \quad (2.4)$$

with $L = 2\pi r$ being the circumference of the ring, n_{eff} the effective refractive index, and λ the wavelength.

From the matrix relation and round trip condition, we get:

$$E_{t1} = t - \alpha t^* e^{-j\theta} \quad (2.5)$$

The effective refractive index n_{eff} is related to the propagation constant β by:

$$\beta = kn_{\text{eff}} = \frac{2\pi n_{\text{eff}}}{\lambda} \quad (2.6)$$

leading to:

$$\theta = \frac{\omega L}{c} = \frac{kc_0 L}{c} = kn_{\text{eff}} \cdot 2\pi r = \frac{4\pi^2 n_{\text{eff}} r}{\lambda}. \quad (2.7)$$

From the matrix relation and the round trip expression, we obtain the throughput port mode amplitude:

$$E_{t1} = t - \alpha e^{j\theta} \left(\frac{\kappa^* \alpha e^{j\theta}}{1 - t \alpha e^{j\theta}} \right). \quad (2.8)$$

2.3.2 Transmission Power

The power transmission at the output waveguide is:

$$P_{t1} = |E_{t1}|^2 = \frac{\alpha^2 + |t|^2 - 2\alpha|t|\cos(\theta + \phi_t)}{1 + \alpha^2|t|^2 - 2\alpha|t|\cos(\theta + \phi_t)} \quad (2.9)$$

where ϕ_t is the phase of the coupler.

The circulating power in the ring is:

$$P_{i2} = |E_{i2}|^2 = \frac{\alpha^2(1 - |t|^2)}{1 + \alpha^2|t|^2 - 2\alpha|t|\cos(\theta + \phi_t)} \quad (2.10)$$

2.3.3 Resonance Condition

At resonance ($\theta + \phi_t = 2\pi m$, where m is an integer), we obtain:

$$P_{t1} = \frac{(\alpha - |t|)^2}{(1 - \alpha|t|)^2}, P_{i2} = \frac{\alpha^2(1 - |t|^2)}{(1 - \alpha|t|)^2} \quad (2.11)$$

At resonance, the output power from the drop port is given by:

$$P_{t2-\text{Resonance}} = |E_{t2-\text{Resonance}}|^2 = (1 - |t_1|^2) \cdot (1 - |t_2|^2) \cdot \alpha (1 - \alpha|t_1 t_2|)^{-2}. \quad (2.12)$$

For identical symmetrical couplers ($t_1 = t_2$) and $\alpha = 1$, indicating full extraction of the resonance wavelength by the resonator, we have:

$$\alpha = |t_1 t_2|. \quad (2.13)$$

If the ring resonator is lossless ($\alpha = 1$), the couplers must be symmetric to achieve minimum intensity at resonance.

2.3.4 Critical Coupling

Critical coupling occurs when the internal losses are equal to the coupling losses ($\alpha = |t|$), resulting in zero transmitted power due to destructive interference. This condition is crucial for achieving high extinction ratios in notch filters.

2.4 Ring Resonator Parameters

2.4.1 Quality Factor

The quality factor (Q factor) is a crucial parameter in ring resonators, indicating the resonator's bandwidth relative to its center frequency. It is given by:

$$Q = \frac{\omega_0}{\Delta\omega} \quad (2.14)$$

where ω_0 is the resonance frequency and $\Delta\omega$ is the bandwidth.

The intrinsic Q factor (without external coupling) can be expressed as:

$$Q_i = \frac{2\pi n_{\text{eff}} r}{\lambda(1 - \alpha)} \quad (2.15)$$

and the loaded Q factor (including coupling effects) as:

$$Q_L = \frac{Q_i}{1 + \left(\frac{\kappa^2}{t^2}\right)}. \quad (2.16)$$

2.4.2 Free Spectral Range

The free spectral range (FSR) is the frequency spacing between successive resonance peaks and is given by:

$$\text{FSR} = \frac{c}{n_{\text{eff}} \cdot L} = \frac{c}{n_{\text{eff}} \cdot 2\pi r}. \quad (2.17)$$

2.5 Notch Filter Characteristics

The wavelength-dependent filter characteristic of a notch-type ring resonator with matched coupling and loss coefficients can be derived from above. The figure below shows the ideal transmission spectrum of a typical notch-type ring resonator filter.

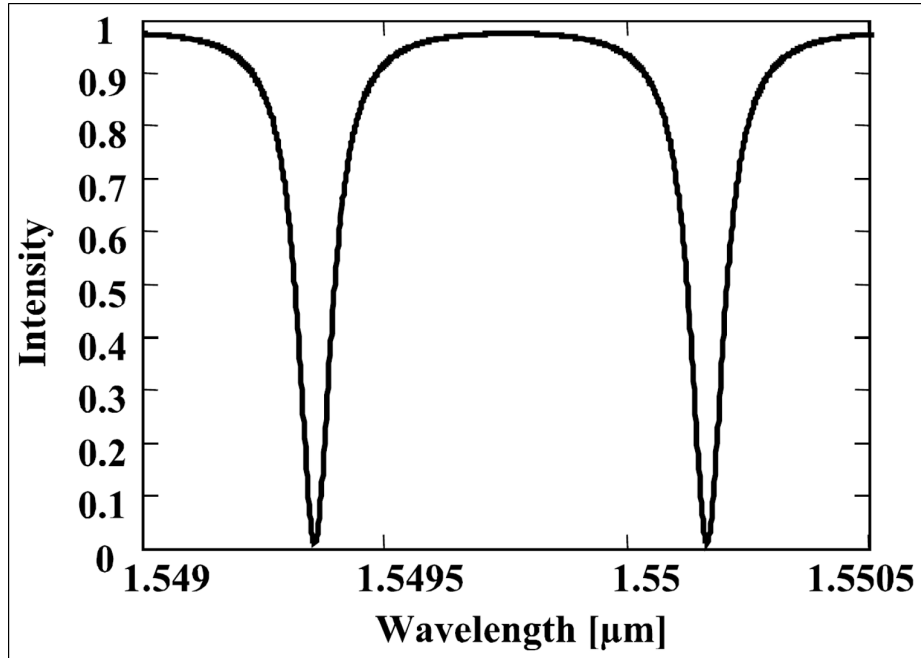


Figure 2.2: Transmission spectrum of a notch-type ring resonator filter

2.6 Simulation Work

Based on the lab's previous work on Notch type Ring Resonators, I had to model and simulate one of the existing works done by the group given in [3]. The dimensions of the structure are as follows:

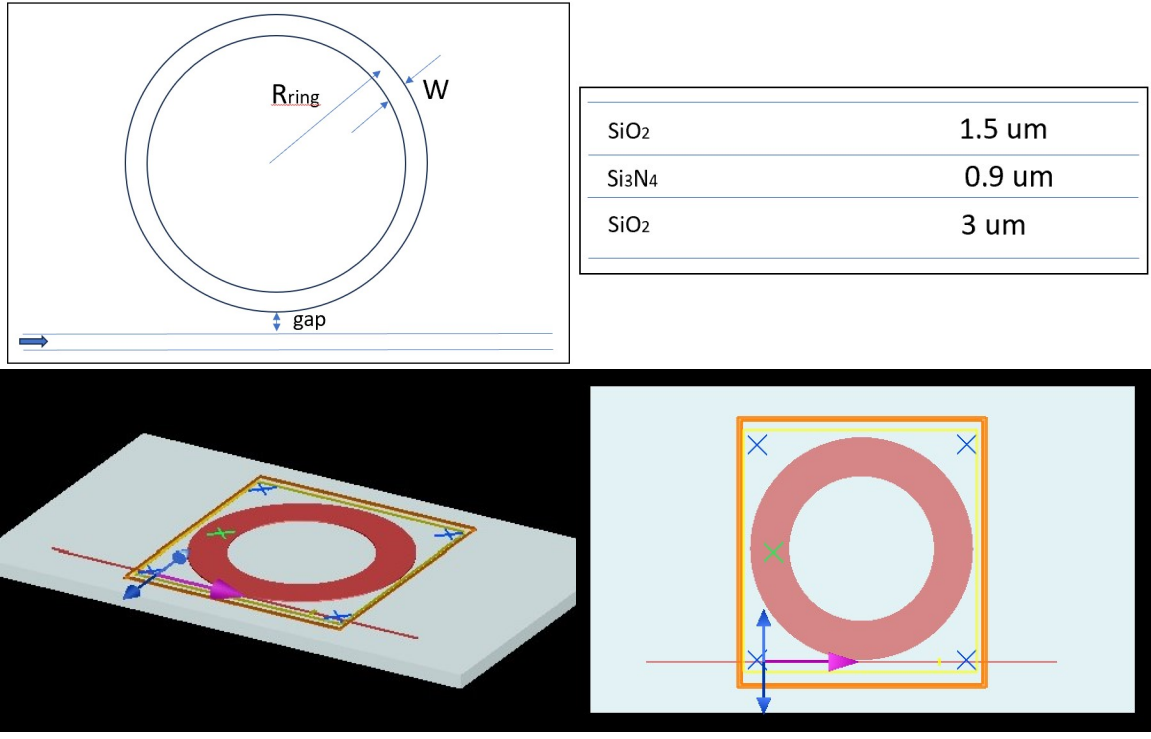


Figure 2.3: Top: Schematic view of the Notch filter ring resonator (Left), Cross Section View (Right). Bottom: Diagram of the simulation on Lumerical FDTD

The physical parameters for the ring:

$$R_{ring} = 55.2 \mu\text{m}, W = 2 \mu\text{m}, \text{gap} = 0.4 \mu\text{m}$$

For the waveguide:

$$\text{Width} = 1.2 \mu\text{m}, \text{Height} = 0.9 \mu\text{m}$$

The material used for them is Si_3N_4 and additionally, there is an SiO_2 cladding on top and bottom of the structure of height 1.5 μm and 3 μm respectively. The TE and TM mode profiles as seen by Eigen Mode analysis on Lumerical FDTD is as follows is satisfactory:

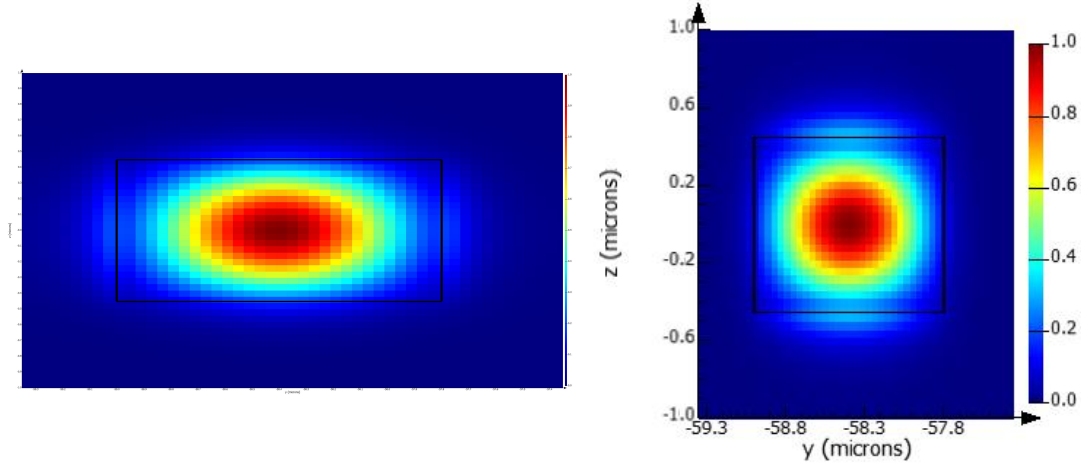


Figure 2.4: Left: TE_{00} mode. Right: TM_{00} mode.

The figure was simulated for the TE_{00} mode and transmission data was collected and analysed for wavelength ranging from 1550 nm to 1558 nm. The data obtained was in accordance with the expected data as per the lab group's previously simulated and experimental data [3].

Chapter 3

Bent Waveguide Ring Resonators

3.1 Structure

Moving upon more advanced version of the Notch type Ring Resonator is the Bent Waveguide Coupled Ring Resonator. The structure for the same is shown below:

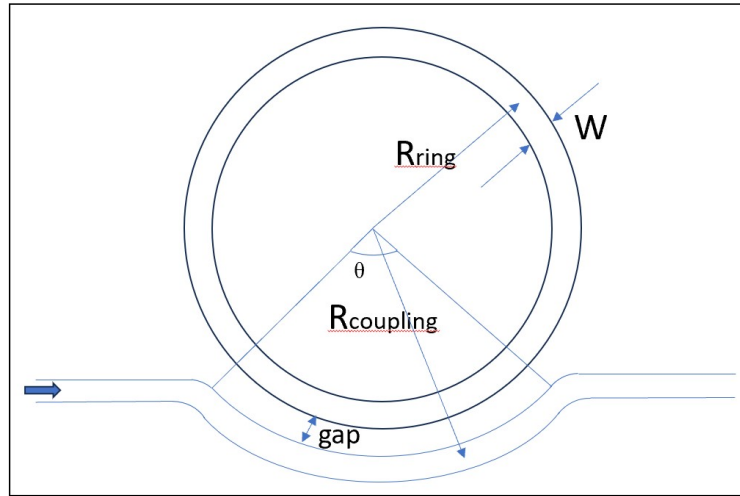


Figure 3.1: Schematic diagram of Bent Waveguide Coupled Ring Resonator

The coupling length (l_c) in this case approximately is equal to $R_{coupling} * \theta$. Material used for the structure is $Al_xGa_{1-x}As$ along with a bottom and top cladding of SiO_2 . I majorly dealt with $x = 0.148$ but the work can be easily extended for other values of x .

[4] talks about the waveguide structures required for making transmitters used in industry standard Telecom Quantum Key Distribution. [4] reported an exceedingly large efficiency for AlGaAs. Inspired from that work, the cross section of this waveguide and the ring is based on the structure used in [4]. It is discussed below:

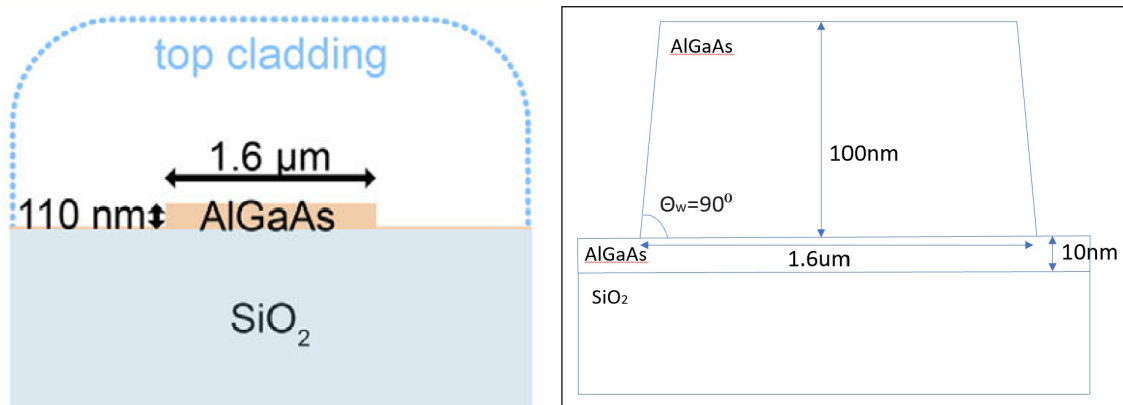


Figure 3.2: Left: Cross Section described in [4] (adopted from [4]). Right: Schematic of the Cross Section used here. Note that θ_w is variable here.

From the figures above, clearly, $R_{coupling} = R_{ring} + gap + W$, $W = 1.6\mu m$. Thus, overall we can alter R_{ring} , gap , $\theta_{coupling}$, θ_{cs} (cross section angle) and x (material). For the time being, we set the following parameters as follows:

Parameter	Value
R_{ring}	50 μm
gap	50 nm
$\theta_{coupling}$	10°
θ_{cs}	90°
x	0.148

3.2 Work Description

My major work was to extract properties of this structure for the TE mode through simulations. Below is the mode profile analysis and comparison with the existing work:

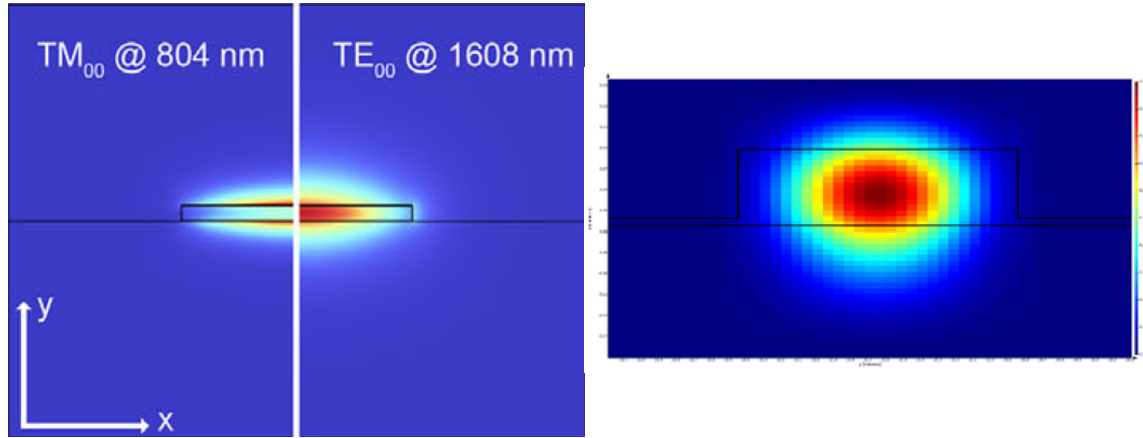


Figure 3.3: Left: TE_{00} and TM_{00} mode profiles for the waveguide as per [4] Right: TE_{00} eigen mode profiles obtained through Lumerical FDTD

Next, I had to find the Transmission data of the ring resonator. The range of wavelengths used was of 30 nm span about 1550 nm centre. In order to maximize the resonance occurrence, now I had to alter the value of the physical parameters (majorly R_{ring} , gap , $\theta_{coupling}$) and find the optimized values that maximize the Q - factor.

The link to the code, entire data and calculations have been provided in the references section.

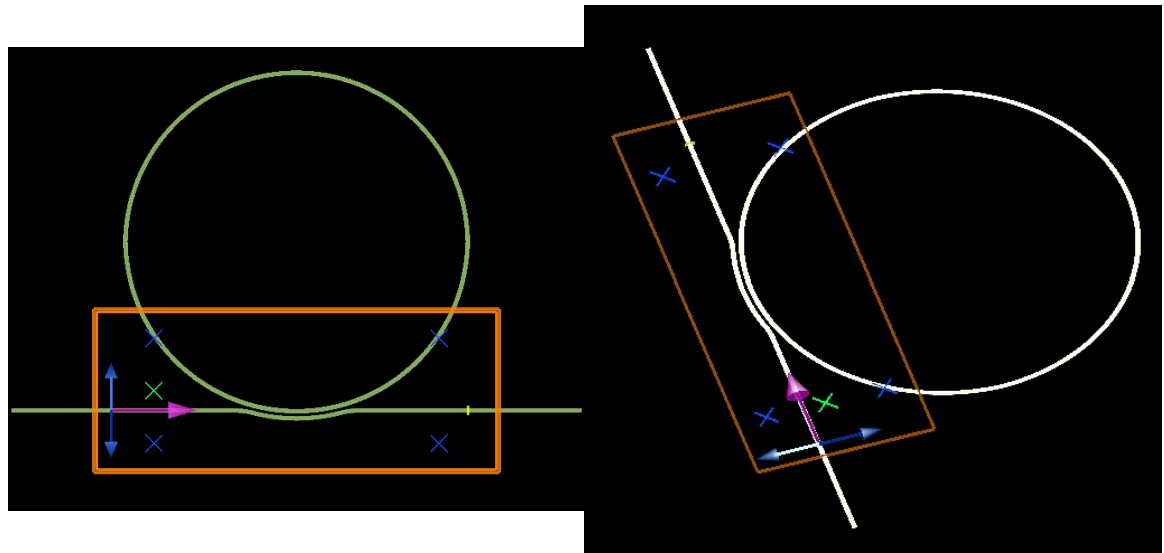


Figure 3.4: Lumerical FDTD Mode setup

3.3 Simulation Results

The link to the code, entire data and calculations have been provided in the references section. The following table summarizes the outputs:

Radius of Ring (μm)	Gap (nm)	Coupling Angle ($^\circ$)	Average Q-Factor
30	50	10	5612
30	100	10	5669
30	120	10	5601
30	150	10	5573
30	100	15	14300
30	100	20	15500
40	100	15	60235
40	100	20	4548
50	100	15	10336
50	100	20	5612
60	100	15	68141

The Q factor is inversely proportional to the effective coupling length ($= R_{coupling} * \theta_{coupling}$). Greater the radius of ring (and hence $R_{coupling}$), lower is the Q factor. Similarly, greater $\theta_{coupling}$ leads to lower Q factor. As per [5], Q factor increases with the gap up to some extent and then decreases as the interference between the waveguides decrease. There is also a variation in the Q factor with the material of waveguide ($Al_xGa_{1-x}As$).

Below is the Electric field profile and the variation of transmission with wavelength for one of the setups:

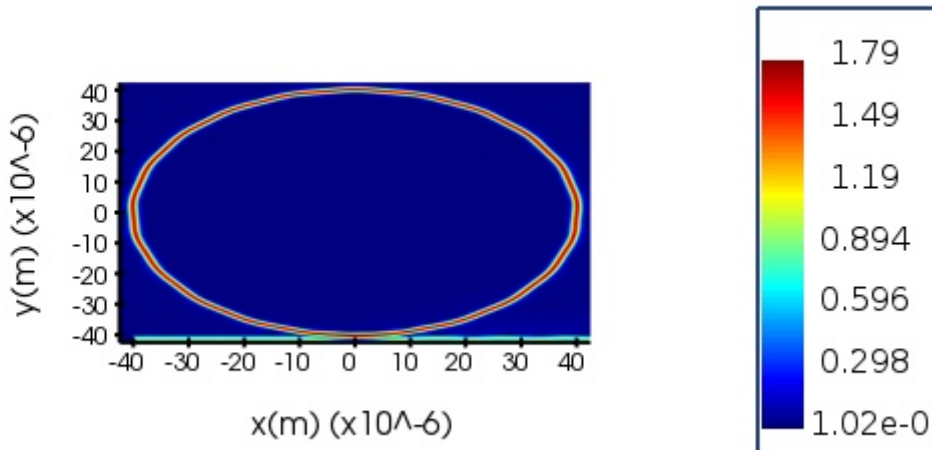


Figure 3.5: Electric Field output profile for TE_{00} mode

3.4 Conclusion and Future Prospects

Keeping in mind the accuracy while fabricating as well as the simulation results, the radius of the ring can be set to $70\mu\text{m}$, gap to 100 nm , the coupling angle can be varied between 10° and 20° . Further optimizations can be performed through altering the cross section height, cross section angle as well as the material of the waveguide to further increase the Q - factor. I was unable to do the TM_{00} mode analysis similar to this TE_{00} mode analysis and try with a material having different value of x . That will give further insights into the optimum parameters for the structure.

[6] suggests a Q - factor of 1.7×10^6 for ridge type waveguide of coupling length $\approx 5\mu\text{m}$. Since, the effective coupling length in our case is much greater, we do expect a smaller Q - factor approximately of the order of 10^5 . Further fine tuning of our parameters would lead to achieving this specified value.

We must also appreciate any discrepancies owing to the fact that different works have calculated Q-factors using different methods and hence, there can be deviations in expected outcomes.

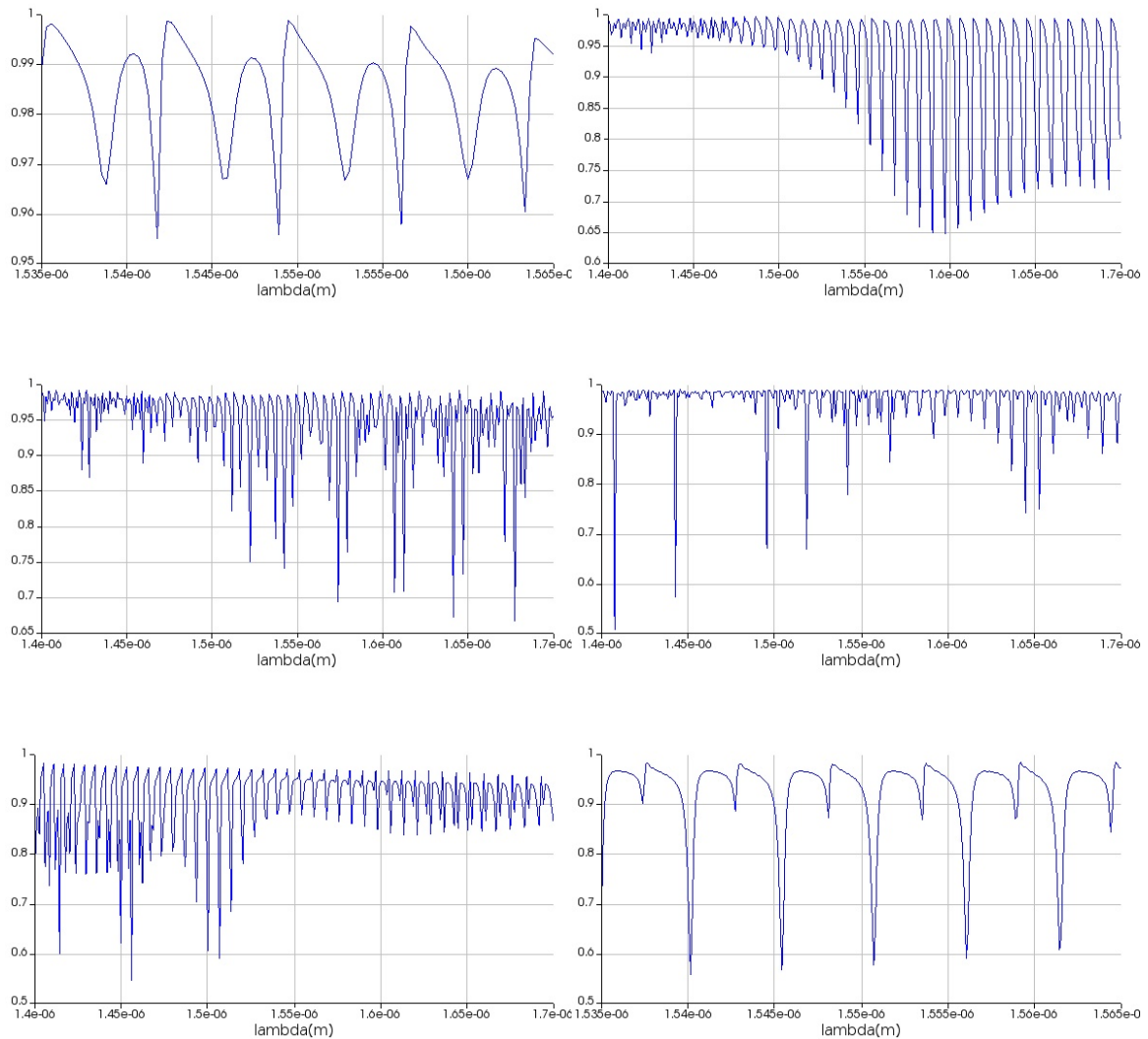


Figure 3.6: Transmission v/s Wavelength plots for different dimensions of the Ring Resonator (refer to references for complete data and codes).

Chapter 4

Utilizing the Voigt Profile for Resonance Curve Fitting in Waveguide Structures

4.1 Introduction

Accurate characterization of resonance curves in waveguide structures is vital for the advancement and optimization of photonic devices. Resonance valleys, occurring at specific wavelengths where transmission significantly drops, offer essential information about the system's properties. Traditional fitting methods, such as Gaussian and Lorentzian profiles, often fall short in accurately depicting these complex shapes.

In the absence of any errors/ broadenings, the curves do resemble Lorentzian profiles. However, random errors leading to Gaussian Broadening push the curves to more Voigt-like shape. The Voigt profile, a convolution of Gaussian and Lorentzian functions, provides a more precise fitting approach by incorporating both inhomogeneous and homogeneous broadening mechanisms. This report explores the Voigt distribution, its application in data fitting, quality factor (Q factor) calculation for transmission data of Bent Waveguide Ring Resonators and comparisons with Gaussian and Lorentzian fits.

4.2 The Voigt Distribution

The Voigt profile is defined as the convolution of a Gaussian function, which accounts for inhomogeneous broadening (e.g., Doppler shifts, instrumental resolution), and a Lorentzian function, which accounts for homogeneous broadening (e.g., natural linewidth, collisional broadening). The Voigt function $V(x; \sigma, \gamma)$ is expressed as:

$$V(x; \sigma, \gamma) = \int_{-\infty}^{\infty} G(x'; \sigma) L(x - x'; \gamma) dx' \quad (4.1)$$

where:

$$G(x; \sigma) = \frac{1}{\sigma\sqrt{2\pi}} \exp\left(-\frac{x^2}{2\sigma^2}\right) \quad (\text{Gaussian function}) \quad (4.2)$$

$$L(x; \gamma) = \frac{\gamma}{\pi(x^2 + \gamma^2)} \quad (\text{Lorentzian function}) \quad (4.3)$$

The parameters σ and γ represent the Gaussian and Lorentzian widths, respectively. The Voigt profile is particularly useful in spectroscopic applications where both types of broadening are present. The Voigt profile takes into account Lorentzian and Gaussian components by the value of the shape index y ($y = \lambda/\gamma$). The capability of Voigt profile is to go through a smooth transition from Gaussian to Lorentzian shape.

4.3 Quality Factor (Q Factor) Calculation

The quality factor Q is a measure of the resonance's sharpness and is defined as the ratio of the resonant frequency to the bandwidth (linewidth) at half-maximum. It is calculated using the formula:

$$Q = \frac{\lambda_0}{\Delta\lambda} \quad (4.4)$$

where λ_0 is the center wavelength, and $\Delta\lambda$ is the full width at half maximum (FWHM). For the Voigt profile, the FWHM is a combination of the Gaussian and Lorentzian widths, providing a more accurate representation of the broadening effects. The FWHM of the Voigt profile can be approximated using the following relation:

$$\Delta\lambda \approx 0.5346 \cdot (2\gamma) + \sqrt{0.2166 \cdot (2\gamma)^2 + (2\sigma)^2} \quad (4.5)$$

This approximation allows for the accurate determination of the Q factor, which is essential for evaluating the performance of resonators

4.4 Data Fitting Using the Voigt Profile

Fitting experimental data with the Voigt profile involves several steps, including data collection, initial parameter estimation, and the use of numerical methods for curve fitting.

4.4.1 Initial Parameter Estimation

Initial guesses for the fitting parameters (amplitude, center wavelength, Gaussian width σ , Lorentzian width γ , offset) are necessary for the fitting algorithm to converge. These guesses can be based on visual inspection or preliminary analyses of the data.

For this discussion, the order of Q-Factor is 10^4 to 10^6 and the wavelengths used for simulation are ranging between 1400 nm and 1700 nm. Thus, a reasonable guess for σ is 10^{-10} and for γ is 10^{-13} . The resonance valleys are detected and the center wavelength is set to the wavelength corresponding to these valleys. Offset is initially set to 0.

4.4.2 Curve Fitting

The Voigt profile can be fitted to the data using nonlinear least squares fitting. Below is a Python example using the `scipy` library.

```
import numpy as np
import matplotlib.pyplot as plt
from scipy.signal import find_peaks
from scipy.optimize import curve_fit
from scipy.special import voigt_profile
from lmfit import Model, Parameters

def load_data(file_path):
    data = np.loadtxt(file_path, delimiter=',')
    wavelength = data[:, 0]
    transmission = data[:, 1]
    return wavelength, transmission

def find_resonance_valleys(wavelength, transmission, distance=3):
    peaks, _ = find_peaks(transmission, distance=distance)
    global_max = max(transmission)
    threshold = global_max / 2
    flt_peaks = [peak for peak in peaks if transmission[peak] >= threshold]
    return flt_peaks

def voigt(x, x0, sigma, gamma, A, offset):
    return A * voigt_profile(x - x0, sigma, gamma) + offset

def fit_voigt_profile(wavelength, transmission, valleys, window_size=20):
```

```

params = []
voigt_model = Model(voigt)
for valley in valleys:
    x0 = wavelength[valley]
    left = max(valley - window_size, 0)
    right = min(valley + window_size, len(wavelength) - 1)

    x_data = wavelength[left:right]
    y_data = 1-transmission[left:right]

    params_init = Parameters()
    params_init.add('x0', value=x0, vary = False)
    params_init.add('sigma', value=1e-14, min = 0)
    params_init.add('gamma', value=1e-11, min = 0)
    params_init.add('A', value=max(y_data))
    params_init.add('offset', value=min(y_data), min = 0)

    result = voigt_model.fit(y_data, x=x_data, params=params_init)
    params.append(result.best_values)

return params

def calculate_q_factors(params):
    q_factors = []
    for p in params:
        lambda_0, sg, gm = p['x0'], p['sigma'], p['gamma']
        fwhm = 0.5346*(2*gm) + np.sqrt(0.2166*(2*gm)**2 + (2.3548*sg)**2)
        q_factor = lambda_0 / fwhm
        q_factors.append(q_factor)
    return q_factors

def main(file_path):
    wl, transmission = load_data(file_path)
    valleys = find_resonance_valleys(wl, 1-transmission)
    params = fit_voigt_profile(wl, transmission, valleys)
    q_factors = calculate_q_factors(params)

    for i, q in enumerate(q_factors):
        print(f"Valley {i + 1}: Q-factor = {q}")
        print(params[i])

    plt.plot(wl, transmission, label='Original Data')
    for p in params:
        plt.plot(wl, 1-voigt(wl, **p), label=f'Voigt Fit (= {(1e9*(p["x0"])):.2f} nm)')
    plt.plot(wl[valleys], transmission[valleys], 'ro', label='Valleys')
    plt.xlabel('Wavelength')
    plt.ylabel('Transmission')
    #plt.legend()
    plt.show()

```

The function `voigt` defines the Voigt profile, which is fitted to the synthetic data `y_data`. The optimized parameters `params` are obtained using the `lmfit` function.

Few of the examples of Voigt fit to the transmission data are as follows (deep blue curve represents the simulated data and the colorful curves are the Voigt profiles fit to each valley locally in its proximity):

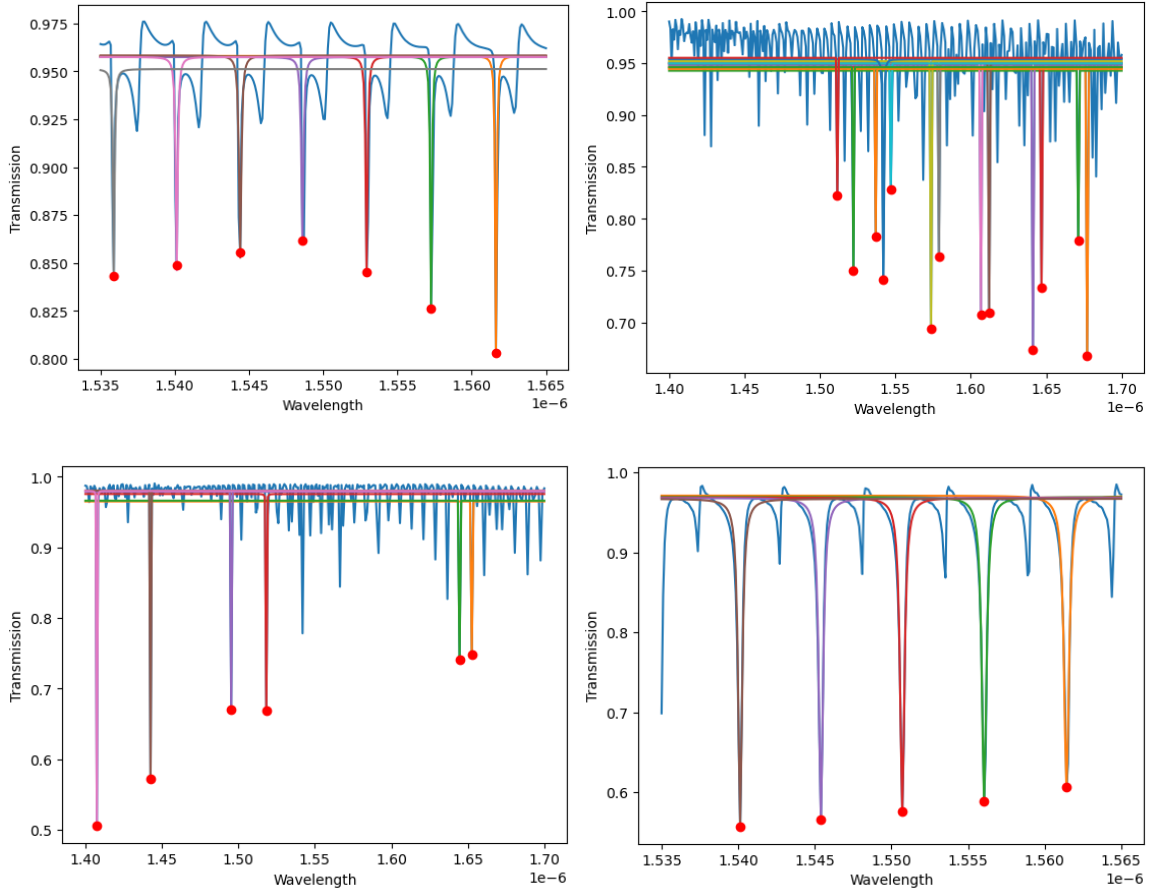


Figure 4.1: Voigt profile fit to the resonance valleys of the transmission data (refer to references for complete data and codes).

4.5 Comparison with Lorentzian and Gaussian Fits

The Voigt profile offers several advantages over Gaussian and Lorentzian fits, particularly in the context of resonance valley fitting in waveguide structures.

4.5.1 Accuracy

The Voigt profile provides a better fit for resonance valleys influenced by both inhomogeneous and homogeneous broadening mechanisms, leading to more accurate parameter estimation. Gaussian and Lorentzian fits, in contrast, often fail to capture the complex shapes of resonance valleys, resulting in less accurate fits.

4.5.2 Parameter Extraction

Using the Voigt profile allows for the extraction of both Gaussian and Lorentzian contributions, offering deeper insights into the underlying physical processes. Single-profile fits (Gaussian or Lorentzian) may misrepresent the actual broadening mechanisms, resulting in less reliable quality factor calculations.

4.5.3 Illustrative Comparison

Below is a Python implementation comparing Voigt, Gaussian, and Lorentzian fits on the same dataset.

```
def gaussian(x, amp, center, sigma):
    return amp * np.exp(-(x - center)**2 / (2 * sigma**2))

def lorentzian(x, amp, center, gamma):
```

```

return amp * gamma**2 / ((x - center)**2 + gamma**2)

# Fit with Gaussian and Lorentzian
popt_gaussian, _ = curve_fit(gaussian, x_data, y_data, p0=[1, 0, 1])
popt_lorentzian, _ = curve_fit(lorentzian, x_data, y_data, p0=[1, 0, 1])

# Plot comparisons
plt.plot(x_data, y_data, label='Data')
plt.plot(x_data, voigt(x_data, *popt), label='Voigt Fit', linestyle='--')
plt.plot(x_data, gaussian(x_data, *popt_gaussian),
label='Gaussian Fit', linestyle=':')
plt.plot(x_data, lorentzian(x_data, *popt_lorentzian),
label='Lorentzian Fit', linestyle='-.')
plt.legend()
plt.xlabel('Wavelength')
plt.ylabel('Transmission')
plt.title('Comparison of Fit Profiles')
plt.show()

```

The code demonstrates how the Voigt profile provides a more accurate fit compared to the Gaussian and Lorentzian profiles.

The Q Factor calculated using Voigt profile seem much more correlating to the results in [6] than just plain Gaussian curve - fitting employed above to show the results in part 1. [7] talks about fitting X-ray spectroscopic data using 3 different methods: Gaussian Lorentzian Sum (GLS), Gaussian Lorentzian Product (GLP) and the Voigt curve. They found that GLS fits their data better than GLP and although Voigt fits the data even better, it is not used due to its computational difficulties.

Most of the Voigt functions available for curve fitting are not the actual Voigt functions but rather the approximations to it. One such approximation is the Voigt–Hjerting function ([8]). The Voigt–Hjerting function is fundamental in order to correctly model the profiles of absorption lines imprinted on the spectra of bright background sources by intervening absorbing systems. [9] uses the Complex Error function to approximate the Voigt profile.

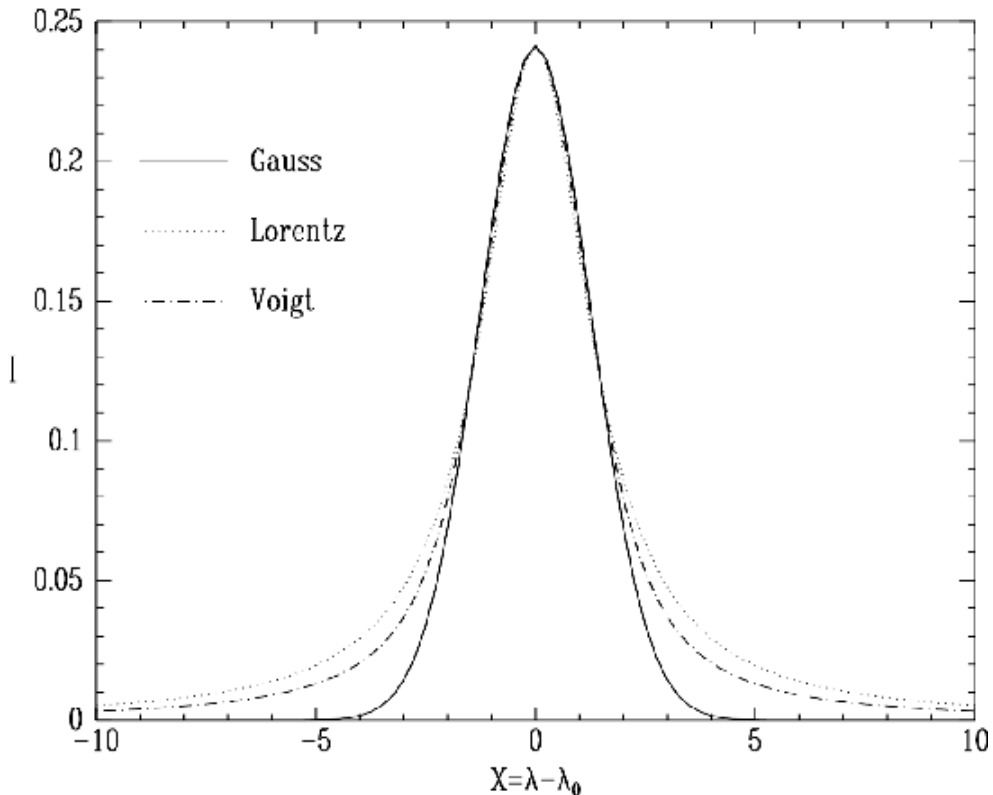


Figure 4.2: Comparing Gaussian, Lorentzian and Voigt profiles. Source: [9]

Above figure shows the differences between fitting the same data to Lorentzian, Gaussian and Voigt profiles. Although all the 3 seemingly coincide at the top of the resonance peaks, an advantage of the Voigt profile is the easy modulation of the "wings" at the bottom unlike Lorentzian and Gaussian profiles.

4.6 Conclusion and Future Prospects

The Voigt profile offers a superior fitting approach for resonance valleys in waveguide structures, providing enhanced accuracy in parameter estimation and quality factor calculation. This leads to a more precise characterization of the resonant features, essential for optimizing the performance of photonic devices. The advantages of the Voigt profile over Gaussian and Lorentzian fits make it a valuable tool in resonance analysis.

Chapter 5

References

- [1] Makarov, D.N. "Fluctuations in the detection of the HOM effect.", Sci Rep 10, 20124 (2020). <https://doi.org/10.1038/s41598-020-77189-6>
- [2] Springer Series in Optical Sciences, ISBN 978-3-030-60130-0, <https://doi.org/10.1007/978-3-030-60131-7>
- [3] Qianni Zhang, Kaiyi Wu, and Andrew W. Poon. "Polarization-entangled sources using waveguide-coupled two-microring-resonators in a silicon nitride platform.", CLEO 2023 © Optica Publishing Group 2023.
- [4] M. Placke, J. Schlegel, F. Mann, P. Della Casa, A. Thies, M. Weyers, G. Tränkle, S. Ramelow, "Telecom-Band Spontaneous Parametric Down-Conversion in AlGaAs-on-Insulator Waveguides.", Laser Photonics Rev 2024, 2301293. <https://doi.org/10.1002/lpor.202301293>
- [5] Islam, Md. Alam, Md. Afsary, Noor Rasel, Md Omar Faruk Ishigure, T.. (2023). "Quality Factor Enhancement Strategies for High-Performance Ring Resonator Sensors.", 10.13140/RG.2.2.22458.16323.
- [6] Bai Mou, Yan Boxia, Qi Yan, Wang Yanwei, Han Zhe, Yuanyuan Fan, Wang Yu, "Ultrahigh Q SOI ring resonator with a strip waveguide.", Optics Communications, Volume 505, 2022, 127437, ISSN 0030-4018, <https://doi.org/10.1016/j.optcom.2021.127437>.
- [7] C.M. Teodorescu, J.M. Esteva, R.C. Karnatak, A. El Afif, "An approximation of the Voigt I profile for the fitting of experimental X-ray absorption data.", Nuclear Instruments and Methods in Physics Research Section A: Accelerators, Spectrometers, Detectors and Associated Equipment, Volume 345, Issue 1, 1994, Pages 141-147, ISSN 0168-9002, [https://doi.org/10.1016/0168-9002\(94\)90983-0](https://doi.org/10.1016/0168-9002(94)90983-0).
- [8] Thorsten Tepper García, "Voigt profile fitting to quasar absorption lines: an analytic approximation to the Voigt–Hjerting function.", Monthly Notices of the Royal Astronomical Society, Volume 369, Issue 4, July 2006, Pages 2025–2035, <https://doi.org/10.1111/j.1365-2966.2006.10450.x>
- [9] Makarov, D.N. "Fluctuations in the detection of the HOM effect.", Sci Rep 10, 20124 (2020). <https://doi.org/10.1038/s41598-020-77189-6>
- [10] John T. Reilly, John M. Walsh, Michael L. Greenfield, Marc D. Donohue, "Analysis of FT-IR spectroscopic data: The Voigt profile.", Spectrochimica Acta Part A: Molecular Spectroscopy, Volume 48, Issue 10, 1992, Pages 1459-1479, ISSN 0584-8539, [https://doi.org/10.1016/0584-8539\(92\)80154-O](https://doi.org/10.1016/0584-8539(92)80154-O).

The detailed codes and results for the work shown in the report can be viewed in:
<https://github.com/NeelRambhia/HKUST-Summer-Intern-2024>